Active Power Filter Under Imbalance and Distortion of Grid Connected Solution

Leminh Thien Huynh[1](✉), Thanh Vu Tran[2], Viet-Dung Do[2], and Van Cuu Ho[1]

[1] SaiGon University, Ho Chi Minh City, Vietnam
[2] University of Transport, Ho Chi Minh City, Vietnam

Abstract. This study proposes an APF grid-connecting solution to reduce harmonic at the moment of connecting transfer status. The work includes analyzing the system structure, the parameters of the passive LCL-filter system, the active power filter (APF) grid-connecting transfer status, the phase lock loop (PLL) for phase-matching connecting algorithms, and the Fuzzy-PI grid connection control based on *d-q* theory. To validate the accuracy of the proposed solution, simulation and experimental results shows that the power system is more stable by applying the transfer of the APF-connecting procedure. The proposed APF grid-connecting also reduces grid current's THD, and matches phase between grid voltage and grid current.

Keywords: Active Power Filter · APF grid connecting · LCL-filter · *d-q* control theory · PI controller · Fuzzy-PI controller · Power quality · PLL · Total Harmonic Distortion

1 Introduction

The electric welding facilities, the increasing of non-linear loads in both consumer electronics in household appliances and semiconductor devices in the factories are the facts that cause the negative effects on power systems, such as high order harmonics, the mismatching phase between grid current and grid voltage, leading low power electric quality and low power factor (PF). In particular, phase imbalance and waveform distortion cause significant total harmonic distortion (THD) [1] and generate high reactive power. Therefore, the power supply system is not fresh anymore, which is the cause of reducing the device's lifespan, increasing the energy consumption of the electronic devices, and lost in energy transmission. To deal with this challenge, the use of Active Power Filter (APF) has been one of the most effective and certified solutions since 1976 in Akagi's research works. Since then, the APF's control technique continuously improved. The p-q theory has been applied for modeling the APF's mathematical architectures of the APF's controller in [3]. In [4–6], the adaptive technique control has been presented to contribute the APF's control methodologies. In [6–8], the grid connecting of the active power filter is obviously required in filtering electrical source, that is also one of the effective solutions for handing out the suitable APF-grid-connecting. Besides, many studies have

N.-S. Vo et al. (Eds.): INISCOM 2021, LNICST 379, pp. 348–366, 2021.
https://doi.org/10.1007/978-3-030-77424-0_29

been promoting to develop the grid-connecting for distributed power systems together [7–13]. However, none of them shows a perfect APF grid-tie-connecting in details, it is needed to develop not only the APF grid-tie-connecting but also the associating of the renewable energy sources to the grid.

In order to improve the efficiency of electrical systems according to IEEE standard STD 519 [14], it is necessary to develop an effective method of APF grid connecting for both source harmonic filters and improving power factor, specially in the period of APF grid-tie-connecting transfering. The grid connecting can inject the APF for the grid-filtering out of high order harmonics from non-linear loads and makes in phase between grid voltage and grid current, but the procedure hardly requires the stability state. So in this study, we first mention about the negative effect of non-linear load on the three-phase grid system. Then, we propose a new solution to match phase for grid voltage called the APF grid-connecting transfering. This connecting transfering procedure aims to improve the stability state of the system as well as reducing the harmonic at the moment of connecting transfer status. The simulation and experiments show that the results of the APF grid-tie-connecting matches the requirements of the IEEE standard STD 519 in terms of the high quality of power, the low delay response and low overshot in the period of connecting transferring. According to IEEE standard STD 519, the total harmonic distortion (THD) is given by:

$$THD = \frac{\sqrt{\sum_{h=2}^{\infty} I_{hRMS}^2}}{I_{RMS}} \tag{1}$$

The rest of this paper is organized as follows. In Sect. 2, the topology of the proposed three-phase APF system working the three-phase grid is presented. In Sect. 3, the control policy in the duty of three-phase grid-tie-connecting is described in details. The simulation and experimental results are shown in Sect. 3.2. Finally, the conclusion is presented in Sect. 4.

2 Three-Phase-APF Grid-Tied-Connecting Control Policy

2.1 Topology of Proposed Three-Phase Grid-Connected APF

Figure 1 shows the configuration of three-phase grid-connected active filter system which consists of an Active Power Filter based on voltage source inverter (VSI-APF), a three-phase LCL-filter, and a three-phase grid with non-linear load. The Active Power Filter consists of the VSI-APF is connected to the three-phase grid system through the LCL-passive filter and the static-transfer-switch (STS).

In order to provide higher frequency harmonic extenuation with the same values of the inductor, we replace a filter made from inductance by a three-phase passive filter. The three-phase passive filter is constructed from an inductance-capacitor-inductance (LCL-filter) as shown in Fig. 1. Because the third-order is caused by the LCL-filter type, an easing of a resistor called R_d is used to eliminate this stability problem. A resistor R_d is defined as a passive damping method. As a result, by using an LCL-filter with APF, the DC link will be working with the reference voltage of 750 VDC with the parameters

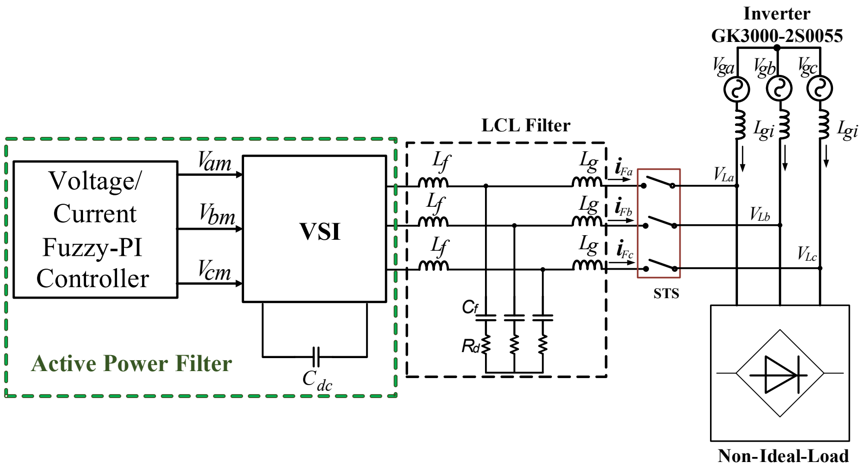

Fig. 1. Configuration of the three-phase grid-connected active filter system.

as follows: the nominal voltage (line-line RMS, $V_{g(ab,bc,ca)} = 220\text{V} \ = \sqrt{3}\ V_{g(a,b,c)}$) is 220 V generated by 5.5 kW single phase (220 V, 50–60 Hz) to the three-phase frequency inverter; model GK3000-2S0055; the output frequency range is 0–400 Hz; L_{gi} is the grid inductance before connecting with Non-Ideal-Load; after creating $V_{(a,b,c)m}$ of the controller, the VSI combines with the LCL-filter to generates i_{Fa}, i_{Fb}, i_{Fc} with 8 kHz of the switching frequency; V_{La}, V_{Lb}, V_{Lc}, are marked at the grid connecting points for three-phase *a, b,* and *c* respectively. STS is the controlled switch or so-called the static-transfer-switch.

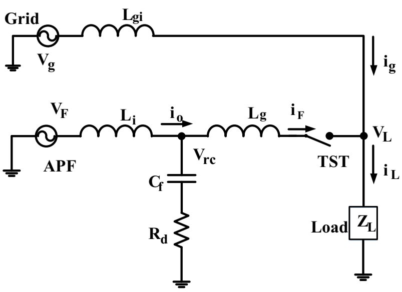

Fig. 2. Equivalent one-phase model.

With a three-phase symmetric system considering in the research, an equivalent one-phase modal can be employed for analysis as shown in Fig. 2. In which the circuit conditions, the base parameters of the system are determined in Table 1.

The LCL-filter is combined with the three-phase grid-connected APF to attenuate the ripples in the APF grid-connecting process. The parameters of the three-phase LCL-filter used in this study are summarized in Table 2.

Table 1. The per-unit system for the circuit condition

Parameters	Calculating	Value
Z_{base}	V^2/P=220^2 / 5000	9.68[Ω]
C_{base}	1/(2πf*Z_{base})=1/2π*50*9.68	328.83[uF]
L_{base}	Z_{base}/2πf=9.68/2π*50	30.816[mH]

Table 2. Summarized list of parameters of the three-phase LCL-filter

Parameters	Value
L_i	1.083[mH]
C_f	12[uF]
L_g	0.2[mH]
R_d	1.5[Ω]

Figure 2 shows the equivalent one-phase model which is the one-phase model of the three-phase grid-connected active filter system in Fig. 1. In Fig. 2, V_F is the output voltage of VSI, i_o is output current of VSI, V_{rc} is the voltage of filter capacitor C_f and small damp resistor R_d in series connection, i_F and V_L are output current and output voltage of stage power conversion, i_L is load current, i_g is the current of the grid, and V_g is the voltage of the grid. The APF inductance L_i and the grid inductance L_g are used as a function of the LCL-filter of the proposed power system. Z_{base} was defined as total equivalent impedance; C_{base} and L_{base} were total equivalent capacitor and total equivalent inductor of the system, respectively.

2.2 The Identification of Scheme

The instability problem of the third order harmonic is caused by an LCL-filter and higher-order harmonics are caused by non-linear loads, the Fuzzy-PI controller was designed to overcome this issue. Some existing works have applied LCL-filters as in [14–18]. In [15, 16], the authors used one extra response or by regulating the ratio of control frequency and the resonance frequency of the LCL-filter. Another work applies the active damping policies for LCL-filters in [17]. The passive damping procedure with a resistor is deployed to overcome the instability problem in [10, 18, 19].

Since the grid form signals and the VSI output form signals are in AC status, they need to be in-phase to make the APF harmonic eliminate function come true. The system negative effects occur suddenly which are the sag-voltage, the current distortion and the delay of calculating in the main controller. Those negative effects may seriously affect the *d-q* calculating result signals from rotation reference. The distortion and imbalance issue can be caused by the transferring from voltage control for the sag-voltage problem to the current control. In [20, 21], the authors associates the controller output current and voltage with the single-phase DGs (Distributed Generations – DGs), however, the

APF output signals with transferring situations need to have an algorithm to adapt with the changing in phase and amplitude of the grid signals.

Figure 3 shows the control loop's scheme of the gird current which consists of the Voltage Fuzzy-PI Controller and Current Fuzzy-PI Controller of the APF. In Fig. 3, the V_{dmc} and V_{qmc} will be the compensate components to reduce THD in the APF-grid-connecting procedure. These signals will be combined with the fixed grid voltage in *d-q* frame, V_{dmv}, and V_{qmv}, to generate V_{dm} and V_{qm} [22].

$$V_{dm} = V_{dmv} + V_{dmc} \tag{2}$$

$$V_{qm} = V_{qmv} + V_{qmc} \tag{3}$$

$$V_{dmc} = \zeta * \Delta V_{gd} + (1 - \zeta)\Delta I_{gd} \tag{4}$$

$$V_{qmc} = \zeta * \Delta V_{gq} + (1 - \zeta)\Delta I_{gq} \tag{5}$$

$$\text{When} \begin{cases} \zeta = 0, V_{g(k)}^{rms} \geq 0.7 * V_g^{rms} \\ \zeta = 1, V_{g(k)}^{rms} < 0.7 * V_g^{rms} \end{cases}$$

The control loop's scheme normally works with the current controller for eliminating high order harmonic, so that $V_{dmc} = \Delta I_{gd}$ and $V_{qmc} = \Delta I_{gq}$. In case of leaking grid voltage; if the magnitude of leaking grid voltage is less than 70% which is defined by the collecting of the *RMS* grid voltage amplitude $k^{th}(V_{g(k)}{}^{(rms)})$, the control loop's scheme will be controlled by the voltage controller denoted as $V_{dmc} = \Delta V_{gd}$ and $V_{qmc} = \Delta V_{gq}$.

In Fig. 2, while getting V_{am}, V_{bm}, and V_{cm} throughout the *d-q* to *abc* converter frame, the VSI plays the role of creating the filter current, $i_F(t)$, to do the active filter function given by:

$$i_F(t) = i_L(t) - i_g(t) \tag{6}$$

By using four Fuzzy-PI controllers instead of the conventional PI controller to get compensated signals, such as $\Delta Vg(d,q) = f_{Fuzzy\text{-}PI}(E_{v(d,q)})$ and $\Delta I_{g(d,q)} = f_{Fuzzy\text{-}PI}(E_{i(d,q)})$ [23], the positive sequence signals in $\alpha\beta$ frame is given by:

$$V_{g\alpha}^{+} = (2/3)^{1/2}\left[V_{ga} - (1/2).\ V_{gb} - (1/2).V_{gc}\right] \tag{7}$$

$$V_{g\beta}^{+} = (1/2)^{1/2}\left[0 + V_{gb} - V_{gc}\right] \tag{8}$$

The phase angle of the grid θ will be calculated by the PLL as in Fig. 4. At first, the $V_{g\alpha}{}^{+}$ and $V_{g\beta}{}^{+}$ are calculated as in (7) and (8), respectively. Then, the PLL use the positive sequence signals of $V_{g\alpha}{}^{+}$ and $V_{g\beta}{}^{+}$ to calculate the exact angle-grid phase.

The phase angle of the grid θ will be calculated by the PLL as in Fig. 4. At first, the $V_{g\alpha}{}^{+}$ and $V_{g\beta}{}^{+}$ are calculated as in (7) and (8), respectively. Then, the PLL use the positive sequence signals of $V_{g\alpha}{}^{+}$ and $V_{g\beta}{}^{+}$ to calculate the exact angle-grid phase. This step aims to synchronize the phase of grid voltage and grid current [24]. The PLL's

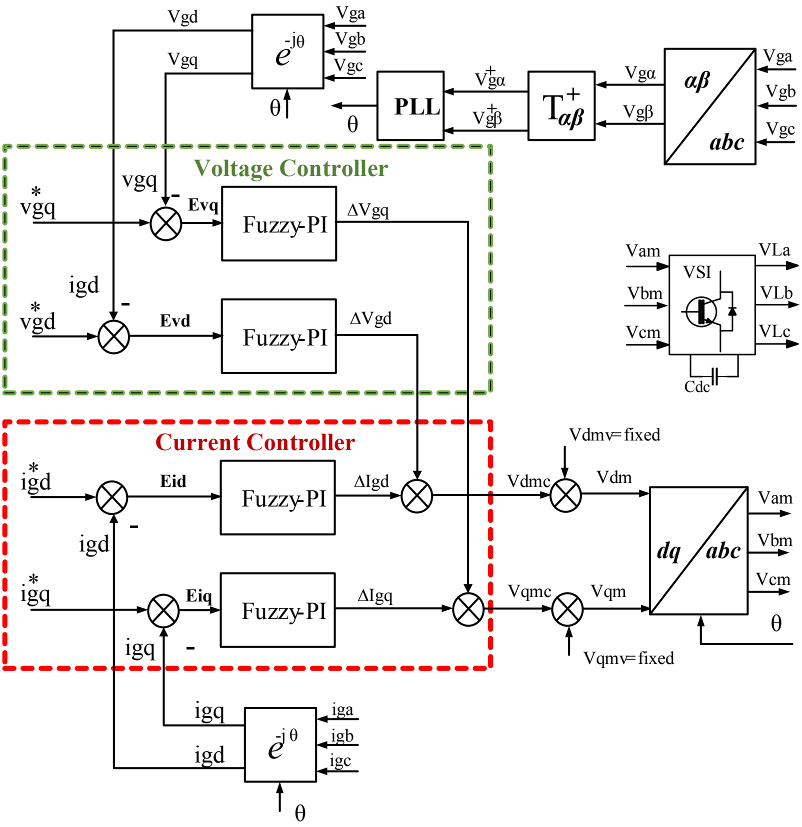

Fig. 3. Control loop's scheme of the grid current.

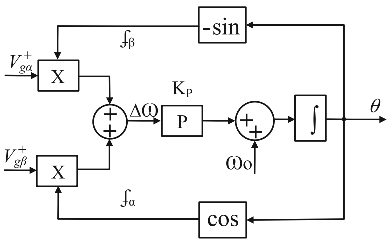

Fig. 4. The block-diagram of PLL controller.

operation applied the d-q theory to generate the θ angle with an unchanging of ωo, shown in Fig. 4. As a result of generating $V_{g\alpha}{}^{+}$ and $V_{g\beta}{}^{+}$, the value of θ is pure which is not affected by high order harmonics.

An angle frequency variation to a phase detector (PD), called Δω, is defined by Eq. (9). Grid voltages' components on a static reference frame in Fig. 3, which consist of $V_{g\alpha}{}^{+}$ and $V_{g\beta}{}^{+}$; the ʃαand ʃβare the sine-feedback and the cosine-feedback of the

PLL's output θ, respectively; $V_P$and θ_P are the original input respectively of voltage and phase.

$$\Delta\omega = V_{g\alpha}{}^{+}.f_{\alpha} + V_{g\beta}{}^{+}.f_{\beta} = V_P sin(\theta_P\text{-}\theta) \tag{9}$$

$$V_{g\alpha}^{+} = \frac{2}{3}V_{gab} - \frac{1}{3}V_{gca} \tag{10}$$

$$V_{g\beta}^{+} = \frac{1}{\sqrt{3}}V_{gbc} \tag{11}$$

By integral calculation of the P-controller output and the feed-forward base angular frequency ω_o, the angle θ is the result from (12), where $\omega_o = 2\pi f_o$.

$$\theta = \int (K_P\Delta\omega + \omega_o)dt \tag{12}$$

2.3 APF in Grid-Tied Operation Mode Control Algorithm

In Fig. 3, the STS connects the three-phase-APF with the LCL-filter to the main grid, the main grid is in normal condition when the STS is closed. The grid current references in *d-q* form can be determined from the expected active and reactive powers as in the conventional PI controller in [25, 26]. The improvement works have applied the Fuzzy-PI controller to adjust the *d-q* APF reference currents [23, 27].

Figure 5 is the structural schematic diagram of the Fuzzy-PI controller in Fig. 3. The conventional PI controller with unchanged K_I and K_P parameters are not convenient for the fast complex instability systems. In [28], a fast adaptive Fuzzy-PI has been applied as in Fig. 5. The parameters in the Fuzzy-PI controller can be listed as follows: the E_μ is the input error; $dE_\mu/d\tau$ is the rate of input deviation; α_μ and α_f are the quantization factor of E_μ and $dE_\mu/d\tau$, respectively; the initialize values for K_I and K_P are $K_I{}^*$ and $K_p{}^*$. The relationship between the two couple parameters (K_I and K_P) and ($dE_\mu/d\tau$ and ΔE_μ) will be estimated by the fuzzy control principle.

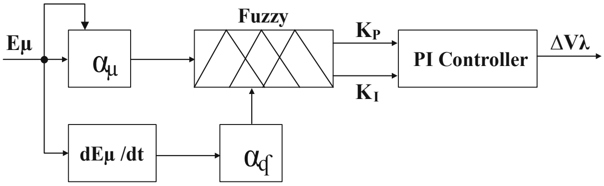

Fig. 5. Fuzzy-PI controller.

In Fig. 5, the Fuzzy-PI controller consists of a Fuzzy controller and a traditional PI controller. The combining of Fig. 3 and Fig. 5 indicates E_μ stands for E_{vq}, E_{vd}, E_{id} and E_{iq}, these signals are the inputs of the Fuzzy-PI; $\Re^*$ and $\Re$ are reference signals and natural signals in *d-q* frame consisting of (v_{gd}^{*}, v_{gq}^{*}), (i_{gd}^{*}, i_{gq}^{*}) and (v_{gd}, v_{gq}), (i_{gq}, i_{gd}) respectively. And certainly ΔV_{λ} represents $\Delta V_{g(d,q)}$ and $\Delta I_{g(d,q)}$.

$$\begin{cases} E_{\mu} = \Re^{*} - \Re \\ dE_{\mu}(\ell)/d\tau = E_{\mu}(\ell) - E_{\mu}(\ell - 1) = \vartheta_{\mu} \\ E_{\mu}(\ell) = E_{\mu}(\ell - 1) \end{cases} \tag{13}$$

After Eqs. (13), furring of E_{μ} and $dE_{\mu}/d\tau$ are done, Mamdani fuzzy rule-based is used to regulate ηK_P and ηK_I.

$$\begin{cases} \eta K_P = \psi_1(E_{\mu}, \vartheta_{\mu}) \\ \eta K_I = \psi_2(E_{\mu}, \vartheta_{\mu}) \end{cases} \tag{14}$$

The results of Eqs. (14) then can be used to determine the proportional K_P and integral coefficients K_I. By that way, the parameters for the PI controller are modified.

$$\begin{cases} K_P = K_P^{*} + \eta K_P \\ K_I = K_I^{*} + \eta K_I \end{cases} \tag{15}$$

Finally, the adjustment signal ΔV_{λ} is calculated through PI controller.

$$\Delta V_{\lambda} = k_p E_{\mu} + k_i \int_0^t E_{\mu} dt \tag{16}$$

In Fig. 5, the *d-q* Fuzzy-PI controllers' outputs is denoted as ΔV_{λ} which consists of ΔI_{gd}, ΔI_{gq}, ΔV_{gd} and ΔV_{gq}. The ΔV_{λ} indicates the grid variation which are supplemented to the fixed *d-q* grid voltages V_{dmv} and V_{qmv} to achieve good dynamic feedback with the grid voltage in feed-forward signals [29].

The phasor diagram in current control mode is shown in Fig. 6. At first, the V_{dmc} and V_{qmc} is calculated by using V_{mc}; then V_m is the addition of V_{dmc} and V_{qmc} which shows the changing of unexpected effecting from the non-linear load. At the transfer's instant from voltage control to current control mode, the outputs signals controller V_{dmc} and V_{qmc} are maintained during the on-grid-connecting operation. The APF output signals in *d-q* format can be controlled by the *d-q* current outputs of controller V_{dmc}, V_{qmc} around the fixed V_{dmv}, V_{qmv} (Fig. 3).

In the current control mode, the synchronization of the output-PLL's angle θ, the angle of grid voltage θ_g, and the α-β voltages' grid can be computed from the sized three-phase-line voltages' grid V_{gab}, V_{gbc}, V_{gca} through Eq. (10) and Eq. (11). In Fig. 7, V_{mc} is the compensating signal, V_{mv} is based on the grid and fixed, and V_m is a sensitive signal caused by an unexpected change of the system. The closed-loop scheme will control the phasor in the voltage control mode while the detecting range of the ${V_g}^{rms}$ is in the range of (0[V], 154[V]). The Fuzzy-PI controller creates V_{dmv} and V_{qmv} by comparing them with the fixed V_{dmc} and V_{qmc} as in Fig. 7. At that time, the same *d-q* reference voltages will be fed to the input voltages of the PLL. The output $\Delta\omega$ will be determined by

$$\Delta\omega = 154 * \cos\theta \cdot (-\sin\theta) + 154 * \sin\theta \cdot \cos\theta \; = \; 0 \tag{17}$$

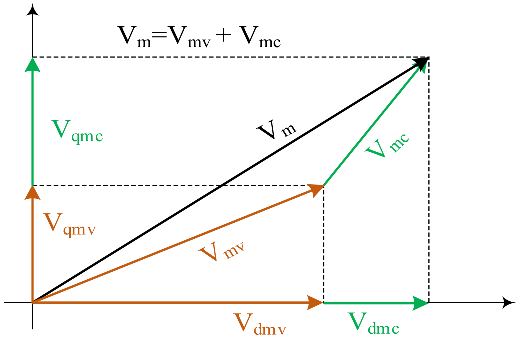

Fig. 6. Phasor diagram in current control mode.

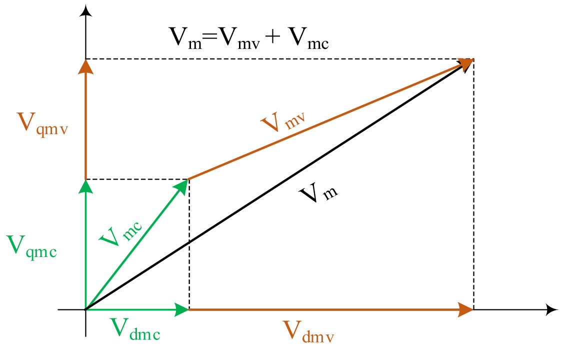

Fig. 7. Phasor diagram in voltage control mode.

Through the Fuzzy-PI control and PLL operation, the VSI can compensate an adding voltage to make getting high quality grid under the sensitive load and imbalance source condition.

3 Simulation and Experience Results

3.1 Simulation Results

In this section, a simulation is conducted using the PSIM program to demonstrate the system with and without the proposed algorithm, also the results of APF grid-connecting algorithm. Non-linear load's effects in a three-phase grid with and without the proposed APF connecting algorithm are shown in Fig. 8.

Figure 9 shows the details of APF-grid-connecting procedure, in which the three-phase load currents have a THD_i of about 30.75% on average with off grid-connecting and the off grid-connecting $THD_{ig(a,b,c)}$ is 30%. In grid-connected time, the grid currents become sine because of reducing high order harmonics, which makes grid currents' $THD_{ig(a,b,c)}$ cutoff to 3.5% in equilibrium. This simulation result indicates the effective working of the APF and the validity of the suggested seamless transfer algorithm.

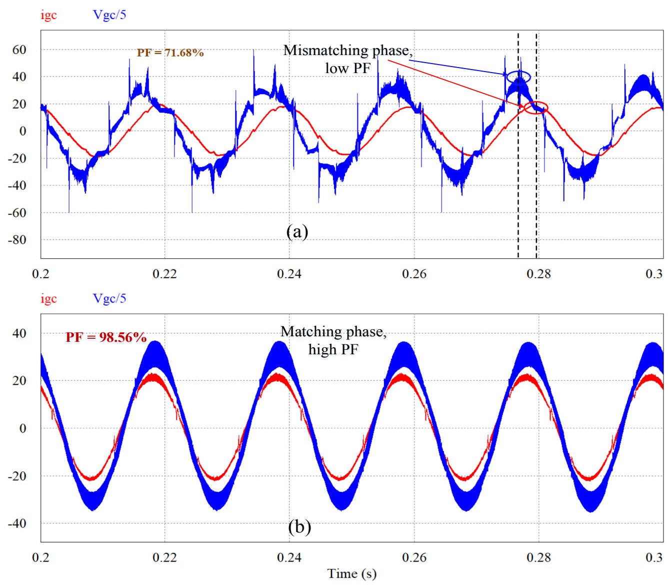

Fig. 8. Simulation results for Non-linear load's effects in three-phase grid: (a) without propose algorithm, mismatch phase between grid current i_{gc} and grid voltage v_{gc}; (b) with propose algorithm, match phase with high PF = 98.56%.

With the proposed algorithm, the synchronization of grid current signal and grid voltage signal is successful matched. Furthermore, when transferring from off grid-connecting to on grid-connecting operation, the in phased of the APF's signals and grid's signals are shown in Fig. 10.

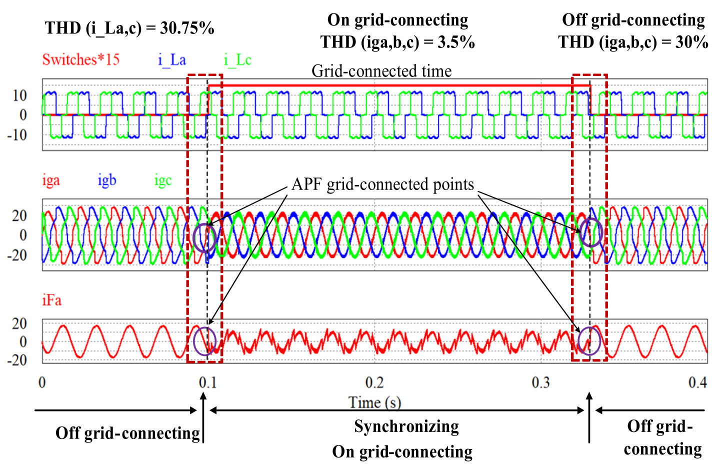

Fig. 9. Simulation results for the proposed algorithm: grid-tie operating procedure.

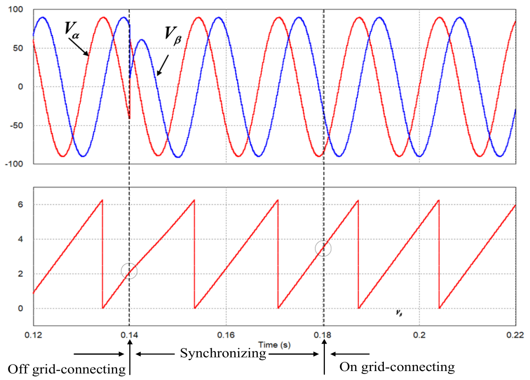

Fig. 10. Simulation results for the proposed algorithm: PLL operation.

Figure 11 shows the results of the transition from on grid-connecting to off grid-connecting operation when there are voltage sag situations in voltage on the main grid. If the $V_g^{(rms)}$ value drops below 70%, the APF recognizes the voltage sags. After regulating the *d-q* grid currents to zero, the STS turns to trip status. Because the compensating voltage mode operation is control by the APF controller, the load voltage is instantly gotten back to the expected voltage.

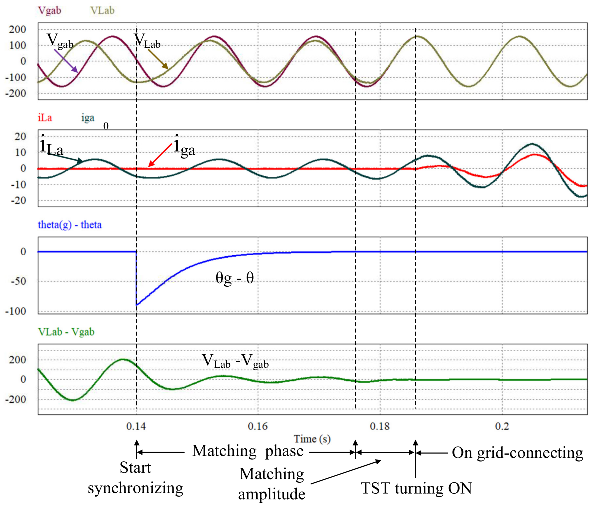

Fig. 11. The results in simulation for the transfer from Off grid-connecting to On grid-connecting with dedicated algorithm: transferring operation mode.

Figure 12 shows the PLL operation at the transition mode. The unbalanced node occurred due to the two-phase voltage sags in α-β grid voltages, the balanced α-β positive sequence voltages are deployed at the input of the PLL controller's voltages. Even though the grid voltage sags exist and in transfer-mode, the PLL controller's angle

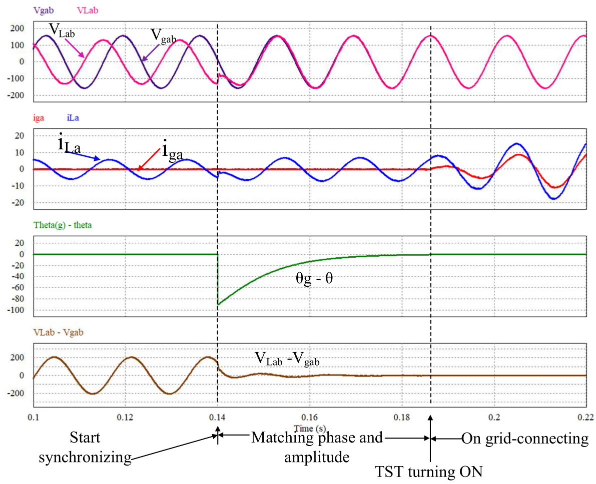

Fig. 12. The results in simulation for the transfer from Off grid-connecting to On grid-connecting operation without dedicated algorithm.

raises without any unexpected jump which is due to the balance of the PLL controller voltage inputs in the α-β reference system.

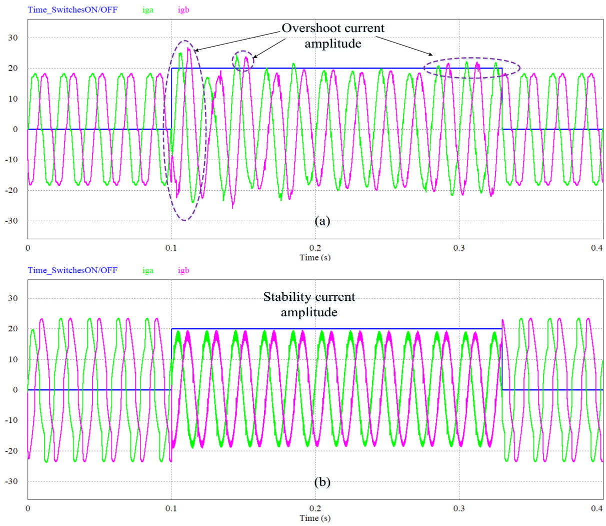

Fig. 13. The results in simulation for the transfer from Off grid-connecting to on grid-connecting operation without dedicated algorithm.

In spite of the little distortion of the load voltage during the short period of time between the sag-voltage occurrence point and the beginning point of the off grid-connecting operation, the APF can transfer evenly to the off-grid mode without the spike-voltages and rush-currents as shown in Fig. 13.

3.2 Experimentation Results

Figure 1 in the Sect. 2 declares the scheme for hardware design with a 5kW three-phase-APF grid-tie-connecting system. The system's controller is conducted by 32-bit STM32H743iiT6. Then, the three-phase-load voltages and grid-side's inductor currents, and three-phase-grid currents and voltages are determined by measurement.

The three-phase switch and the two IGBTs per phase are in anti-serial are considered as the STS, and an on-grid/off-grid signal for STS is created by the controller. A programmable three-phase source is applied to imitate the main grid such as sag-voltage existing. Figure 14 shows the in phase of the output VSI voltage and the grid voltage.

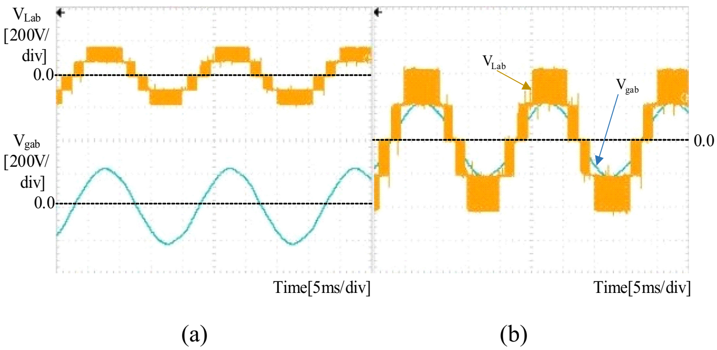

Fig. 14. Grid-tied operation experimental results with proposed algorithm: (a) grid voltage V_{gab} and VSI voltage V_{Lab}. (b) In phase of the two signals.

Figure 15 and Fig. 16 show the experimental signals when the system working in changing from on grid-connecting to off grid-connecting operation (Fig. 15) and the working's result of the PLL (Fig. 16) with the suggested algorithm.

Figure 17 and Fig. 18 show the results of experimentation for the transferring from on grid-connecting to off grid-connecting operation under a sag-voltage of 70% in the main grid during the on grid-connecting operation. In Fig. 17, after tripping STS, the load voltage immediately obtains its expected voltage at the off grid-connecting operation

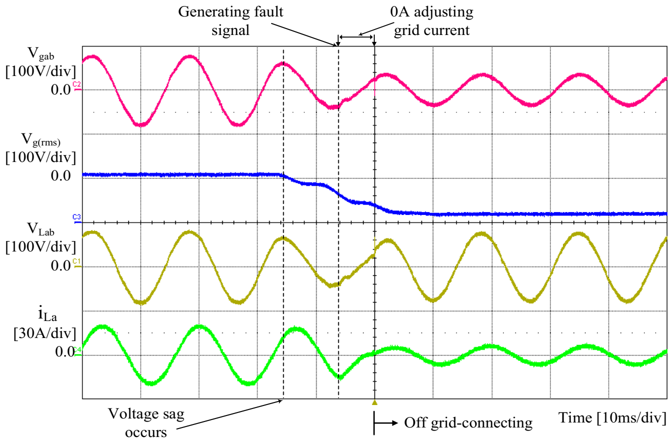

Fig. 15. Experimental results for the transfer from on-grid-connecting to off-grid-connecting operation with proposed algorithm: grid voltage and output voltage and current.

mode, the currents in *d-q* reference and also the current of a-phase-grid are regulated to zero before the STS turns to trip status. Figure 18 shows the input voltages' balanced in the α-β reference system and the synchronization of PLL's angle, which raises evenly during the sag-voltage and the transferring-mode.

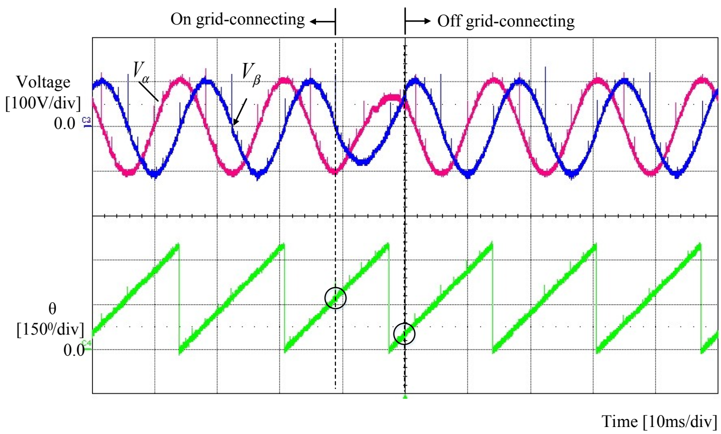

Fig. 16. Experimental results for the transfer from On-grid-mode to Off-grid-mode with proposed algorithm: PLL operation.

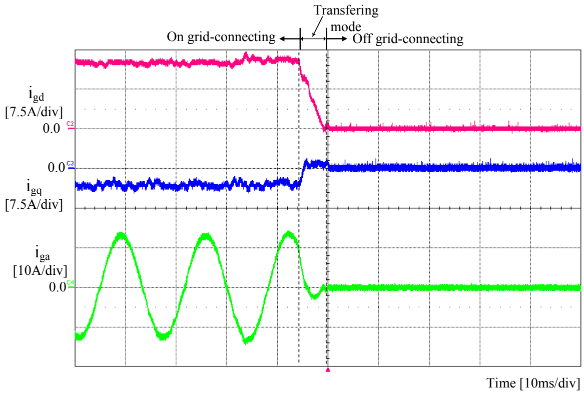

Fig. 17. The results of experimentation for the transferring status from on grid-connecting to off grid-connecting operation with suggested algorithm: d-q grid currents.

Figure 19 shows the results of experimentation for the transfer from off grid-connecting to on grid-connecting operation with the proposed algorithm: grid and load voltages. Figure 20 points out the results of experimentation for the transfer from off grid-connecting to on grid-connecting operation with the suggested algorithm with the signs of grid current and load currents. It is obvious that the result has low quality when the system works without the proposed algorithm (Fig. 21).

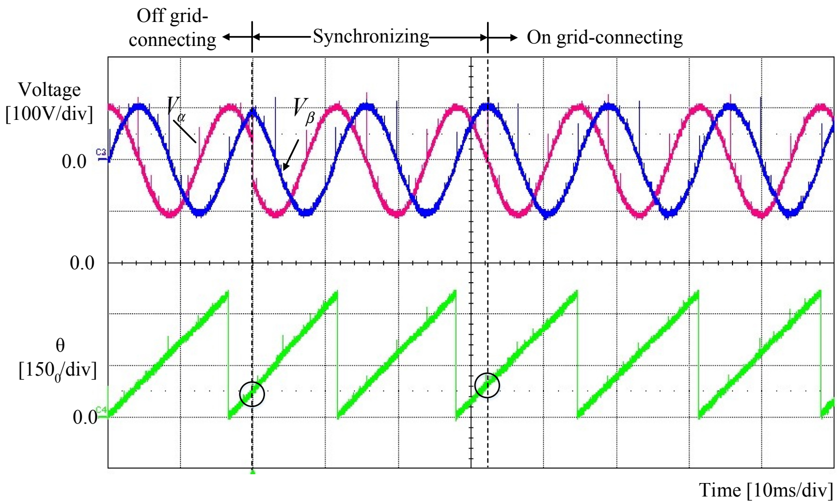

Fig. 18. The results of experimentation for the transferring status from off grid-connecting to on grid-connecting operation with suggested algorithm: the operation of PLL.

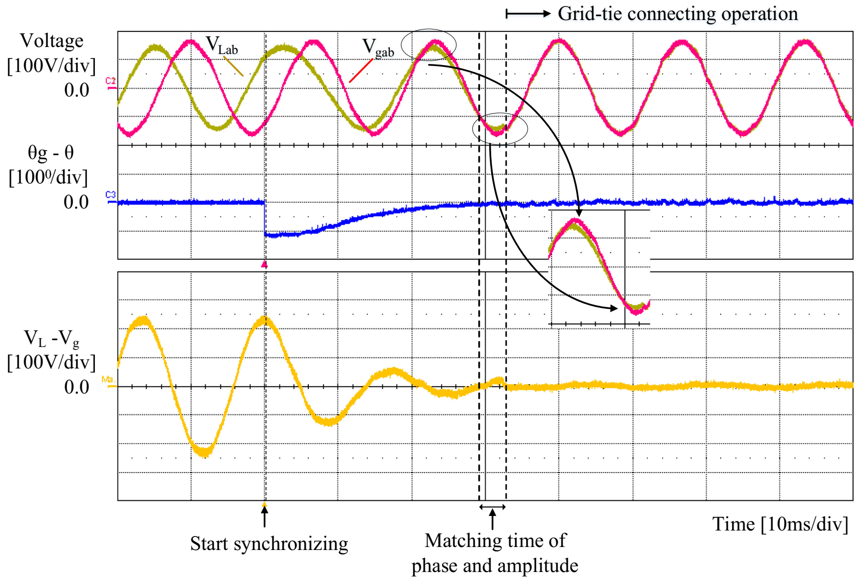

Fig. 19. The results of experimentation for the transferring status from off-grid-connecting to on-grid-connecting operation using proposed algorithm: grid-voltages and load-voltages.

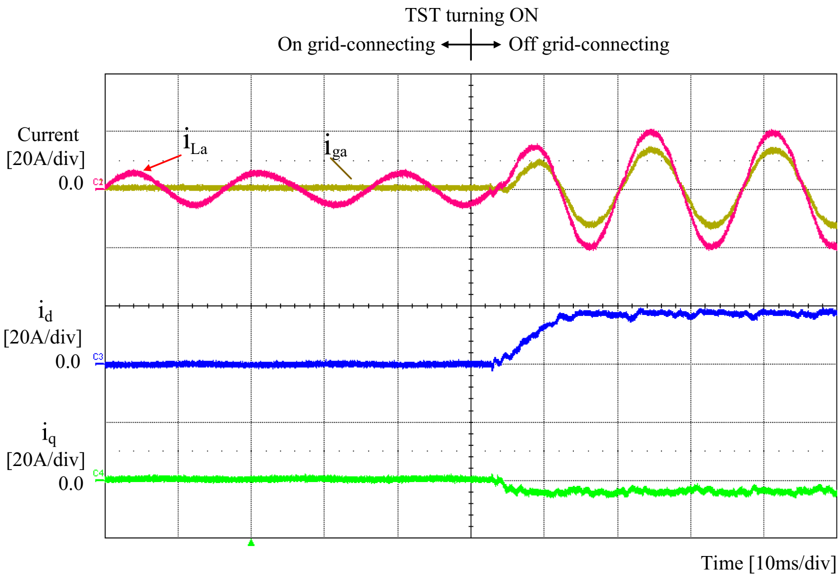

Fig. 20. Experimental results for the transfer from off-grid-connecting to on-grid-connecting operation with proposed algorithm: grid and load currents.

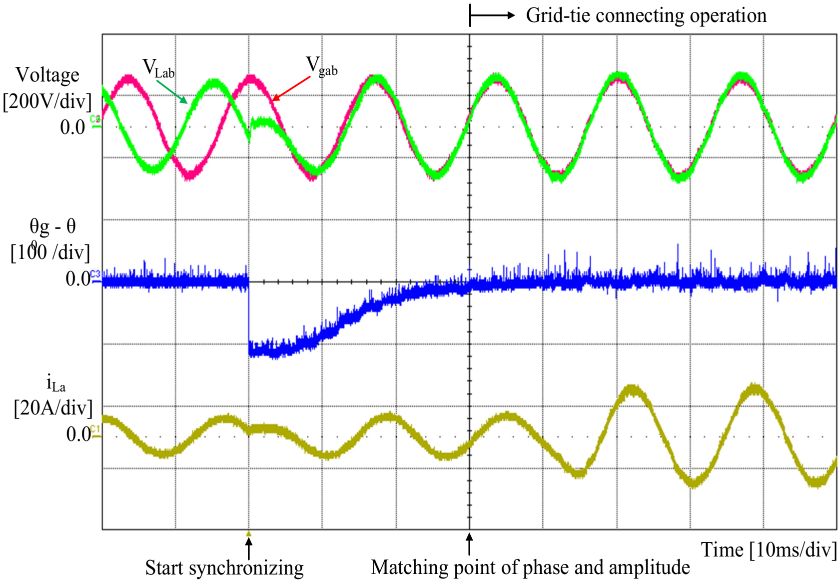

Fig. 21. Experimental results for the transfer from off-grid-connecting to on-grid-connecting operation without proposed algorithm.

4 Conclusion

After simulating the proposed algorithm in Psim software, the experiment in the active power filter hardware system using the STM32H743iiT6 microcontroller chip has been completed. With the results obtained, besides matching phase for grid current and grid voltage to increase power factor and eliminating high order harmonics to decrease THDi from 30.07% to 3.5%, it is seen that the magnitude of the load voltage and its phase are successively matched to the grid-voltage without any distortion and spike. Also, with the proposed algorithm, the active power filter's signals and the grid's ones have in-phase and equivalent values in amplitude, reducing the instantaneous overshot current amplitude at the time of the APF on grid transferring. In the future, this model can be improved to work with serious sag-voltage in the time of over tens fundamental cycle by using ultra-capacitor instead of C_{dc}-link.

References

1. Suhendar, Firmansyah, T., Maulana, A., Zuldiag, Dewanto, V.: Shunt active power filter based on P-Q theory with multilevel inverters for harmonic current compensation. Telkomnika (Telecommun. Comput. Electron. Control) **15**(4), 1632–1640 (2017)
2. Ucar, M., Ozdemir, E.: Control of a 3-phase 4-leg active power filter under non-ideal mains voltage condition. Electr. Power Syst. Res. **78**(1), 58–73 (2008)
3. Dang, X.K., Do, V.D., Nguyen, X.P.: Robust adaptive fuzzy control using genetic algorithm for dynamic positioning system. IEEE Access **8**(December), 222077–222092 (2020)

4. Do, V.-D., Dang, X.-K., Huynh, L.-T., Ho, V.-C.: Optimized multi-cascade fuzzy model for ship dynamic positioning system based on genetic algorithm. In: Duong, T.Q., Vo, N.-S., Nguyen, L.K., Vien, Q.-T., Nguyen, V.-D. (eds.) INISCOM 2019. LNICSSITE, vol. 293, pp. 165–180. Springer, Cham (2019). https://doi.org/10.1007/978-3-030-30149-1_14
5. Do, V., Dang, X.: Fuzzy adaptive interactive algorithm design for marine dynamic positioning system under unexpected impacts of Vietnam Sea. Indian J. Geo Mar. Sci. **49**(November), 1764–1771 (2020)
6. Zeng, Z., Yang, H., Zhao, R., Cheng, C.: Topologies and control strategies of multi-functional grid-connected inverters for power quality enhancement: a comprehensive review. Renew. Sustain. Energy Rev. **24**, 223–270 (2013)
7. Kamel, R.M.: New inverter control for balancing standalone micro-grid phase voltages: a review on MG power quality improvement. Renew. Sustain. Energy Rev. **63**, 520–532 (2016)
8. Mahmud, N., Zahedi, A.: Review of control strategies for voltage regulation of the smart distribution network with high penetration of renewable distributed generation. Renew. Sustain. Energy Rev. **64**, 582–595 (2016)
9. Santoso, H., Budiyanto, B.: Microgrid development using a grid tie inverter. MAKARA J. Technol. Ser. **17**(3), 121–127 (2014)
10. Eren, S.: Composite nonlinear feedback control and stability analysis of a grid-connected voltage source inverter with LCL filter. IEEE Trans. Ind. Electron. **60**(11), 5059–5074 (2013)
11. Zhang, X., Wang, Y., Yu, C., Guo, L., Cao, R.: Hysteresis model predictive control for high-power grid-connected inverters with output LCL filter. IEEE Trans. Ind. Electron. **63**(1), 246–256 (2016)
12. Singh, M., Chandra, A.: Real-time implementation of ANFIS control for renewable interfacing inverter in 3P4W distribution network. IEEE Trans. Ind. Electron. **60**(1), 121–128 (2013)
13. Hoevenaars, T., LeDoux, K., Colosino, M.: Interpreting IEEE STD 519 and meeting its harmonic limits in VFD applications. In: Record of Conference Papers - Annual Petroleum and Chemical Industry Conference, pp. 145–150 (2003)
14. Guzman, R., De Vicuna, L.G., Morales, J., Castilla, M., Miret, J.: Model-based control for a three-phase shunt active power filter. IEEE Trans. Ind. Electron. **63**(7), 3998–4007 (2016)
15. Vodyakho, O., Mi, C.C.: Three-level inverter-based shunt active power filter in three-phase three-wire and four-wire systems. IEEE Trans. Power Electron. **24**(5), 1350–1363 (2009)
16. Hogan, D.J., Gonzalez-Espin, F., Hayes, J.G., Lightbody, G., Egan, M.G.: Adaptive resonant current-control for active power filtering within a microgrid. In: 2014 IEEE Energy Conversion Congress and Exposition, ECCE 2014 (2014)
17. Zammit, D., Spiteri Staines, C., Apap, M., Licari, J.: Design of PR current control with selective harmonic compensators using Matlab. J. Electr. Syst. Inf. Technol. **4**, 347–358 (2017)
18. Srinath, S., Poongothai, M.S., Aruna, T.: PV integrated shunt active filter for harmonic compensation. Energy Proc. **117**, 1134–1144 (2017)
19. He, J., Li, Y.W., Blaabjerg, F., Wang, X.: Active harmonic filtering using current-controlled, grid-connected DG units with closed-loop power control. IEEE Trans. Power Electron. **29**(2), 642–653 (2014)
20. Tran, T.V., Chun, T.W., Lee, H.H., Kim, H.G., Nho, E.C.: PLL-based seamless transfer control between grid-connected and islanding modes in grid-connected inverters. IEEE Trans. Power Electron. **29**, 5218–5228 (2014)
21. Leminhthien, H., Thanhvu, T., Vancuu, H.: The effecting of non-ideal-load on three-phase-power systems using fuzzy control active power filter. J. Transp. Sci. Technol. **27+28**, (05/2018), 119–121 (2018)
22. Thien, H.L.M., van Huong, D., Tien, N.X., van Cuu, H., Vu, T.T.: Improving the electric quality of the back-to-back system on modern electric railways using active power filter algorithm. J. Mech. Eng. Res. Dev. **44**(1), 83–98 (2020)

23. Karuppanan, P., Mahapatra, K.K.: PLL with fuzzy logic controller based shunt active power filter for harmonic and reactive power compensation. In: India International Conference on Power Electronics, IICPE 2010 (2011)
24. Van, T.L., Huynh, L., Tran, T.T., Nguyen, D.C.: Improved control strategy of three-phase four-wire inverters using sliding mode input-output feedback linearization under unbalanced and nonlinear load conditions (2015)
25. Trinh, Q.-N., Lee, H.-H.: An advanced current control strategy for three-phase shunt active power filters. IEEE Trans. Ind. Electron. **60**(12), 5400–5410 (2013)
26. Dehini, R., Benachaiba, C.: Improving the active power filter performance by robust self-tuning face to sudden change of load. J. Electr. Eng. 1–9 (2020)
27. Pitalúa-Díaz, N., Herrera-López, E.J., Valencia-Palomo, G., González-Angeles, A., Rodríguez-Carvajal, R.A., Cazarez-Castro, N.R.: Comparative analysis between conventional PI and fuzzy logic PI controllers for indoor Benzene concentrations. Sustainability **7**(5), 5398–5412 (2015)
28. Bouzelata, Y., Kurt, E., Altin, N., Chenni, R.: Design and simulation of a solar supplied multifunctional active power filter and a comparative study on the current-detection algorithms. Renew. Sustain. Energy Rev. **43**, 1114–1126 (2015)